Medicinal Chemistry Research (2019) 28:1471–1487
https://doi.org/10.1007/s00044-019-02387-5

MEDICINAL CHEMISTRY RESEARCH

ORIGINAL RESEARCH

Novel chromenes and benzochromenes bearing arylazo moiety: molecular docking, in-silico admet, in-vitro antimicrobial and anticancer screening

Tarek H. Afifi[1] · Sayed M. Riyadh[1,2] · Anwar A. Deawaly[1] · Arshi Naqvi[1]

Received: 30 March 2019 / Accepted: 19 June 2019 / Published online: 28 June 2019

Abstract

Novel derivatives of benzochromene **9a–e** and chromene **10a–e** were synthesized via multi components reaction that utilizes azo dyes, malononitrile, and arylaldehydes as starting materials. The structures of the newly synthesized compounds were elucidated by the IR, ^{1}H-NMR, ^{13}C-NMR and mass spectral data. The new synthesized compounds were explored for their in-silico ADMET properties. The docking investigations verified good docking outcomes in terms of score and binding affinities of the examined compounds on the desired proteins, namely the GlcN-6-P synthase and PI3Ks. The in-vitro studies, which encompassed the antibacterial activity against two types of Gm +ve and two of Gm –ve, and the antifungal activity against four fungi micro-organisms were evaluated by the well diffusion method for the synthesized compounds. Moreover, the anticancer activity was tested against three human carcinoma cell lines [human colon carcinoma (HCT-116), human breast adenocarcinoma (MCF-7), and liver carcinoma (HEPG-2)], exhibiting promising anticancer activity in comparison to Vinblastine, Colchicine and Doxorubicin as standard drugs. The data suggests that some of the new derivatives of chromene scaffold which emerged promising in the in-silico molecular docking studies displayed good in-vitro antimicrobial and anticancer activities and could be exploited as leads for further optimization.

Keywords Arylazochromene · Anticancer activity · Antimicrobial Activity · In-silico screenings

Introduction

Chromene has been explored as a privileged structure, which can be identified in synthetic medicinal chemistry as a single molecular framework able to provide ligands for diverse receptors (Atta-ur-Rahman and Thomsen 2001). The majority of researches have been centered on the development of 2-amino-4*H*-chromene and their derivatives. These compounds have been recognized as ideal medicinal scaffolds because of their unique pharmacological and biological activities, as antibacterial (Ali et al. 2015) and/or anticancer agents (Cai et al. 2006). In addition, chromene demonstrates several other incredible applications, including: antileishmanial (Foroumadi et al. 2010; Tanaka et al. 2007), antioxidant (Fadda et al. 2012 ; Nareshkumar et al. 2009), vascular-disrupting (Kasibhatla et al. 2004), blood platelet antiaggregating (Lee et al. 2006), analgesic and hypolipidemic effects (Sashidhara et al. 2011). Furthermore, the appliance of these moieties for disease therapy and for the enhancement of potent antitumor agents has presented efficacious models in literature. For instance, Crolibulin™ (**A**) is currently in phase I/II of clinical trials for the treatment of advanced solid tumors (Tiana et al. 2008; Hermanson et al. 2009). 2-Amino-4-(3-bromo-4,5-dimethoxyphenyl)-7-(dimethylamino)-4*H*-chromene-3-carbonitrile (**B**) has been known as a tubulin inhibitor (El-Agrody et al. 2014) (Fig. 1).

The synthetic methodology of chromenes has been accomplished over the years, employing various pathways, such as multicomponent reactions (MCRs) (Kirilmis et al. 2008; Elinson et al. 2010; Hosseini-Sarvari and Shafiei Haghighi 2011; Boominathan et al. 2011), heterogeneous catalytic methods (Mehrabi and Kazemi-Mireki 2011; Yadav

✉ Tarek H. Afifi
afifith@yahoo.com

[1] Department of Chemistry, Faculty of Science, Taibah University, 30002 Al-Madinah Al-Munawarah, Saudi Arabia

[2] Department of Chemistry, Faculty of Science, Cairo University, Giza 12613, Egypt

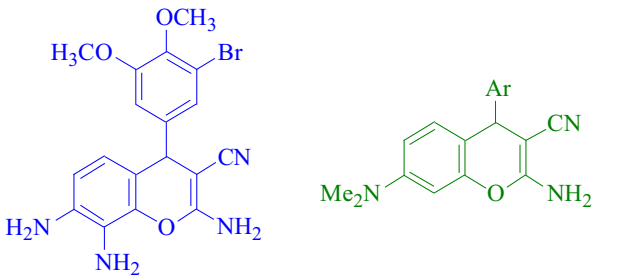

(**A**) Crolibulin

(**B**) MX58151
Ar = 3-Br-4,5-$MeOC_6H_2$

Fig. 1 Chromene compounds with promising biological activities

et al. 2007), electro catalytic procedures (Makarem et al. 2008), microwave and ultrasound techniques (Hamelin et al. 2002; Zbancioc and Mangalagiu 2006; Bejan and Mantu 2012; Zbancioc and Zbancioc 2014; Safari and Javadian 2015). Among these strategies, multicomponent reactions (MCR) are deemed as one of the most effective routes due to the simplicity of usage, low cost, and the production of a sufficient yield of the desired product. The combination of the chromene derivatives with the azo dyes hadn't gained the attentiveness of scientists even though the chromene scaffold appears to be an attractive precursor for the formation of novel azo chromophores. Recently, we reported the first model of chromene, containing azo chromophores, and investigated their biological properties. As a continuation to our preceding work (Afifi et al. 2017), herein we introduce the synthesis and characterization of a novel series of azo chromophores with chromene moieties. The synthesized compounds were investigated for their pharmacodynamic and pharmacokinetic properties via in-vivo ADMET (absorption, distribution, metabolism, excretion and toxicity) predictions. Moreover, the chromene derivatives have been reported as glucosamine-6-phosphate synthase (GlcN-6-P synthase) and Phosphoinositide 3-kinases (PI3Ks) inhibitors (Govori et al. 2017; Chen-Chen M and Zhao-Peng 2016; Cheng et al. 2003; Mao et al. 2011). In this regard, the in-silico molecular docking screenings are employed mainly to understand the drug-receptor interaction. Along with these in-silico studies, this work also incorporates the screening of the biological features of the targeted compounds.

Results and discussion

Chemistry

The diazotization of aniline derivatives [4-toludine (**1a**) and 4-aminoacetophenone (**1b**)] or [(2-amino-5-substitutedphenyl) (phenyl)methanone] (**4a**, **b**) in the presence of nitrous acid at 0–5 °C afforded the corresponding diazonium salts. The coupling reaction of these diazonium salts with the phenolic components, containing reactive hydrogen atom(s) such as, 2-naphthol or resorcinol, led to the formation of the azo dyes **3a**, **b** or **6a**, **b**, respectively (Scheme 1). The structure identities of the obtained azo dyes were deduced from their spectral analysis. For example, the infrared spectra of these products showed the appearance of the absorption band at 1450–1446 cm^{-1}, which is a characteristic of the azo group (N = N). Meanwhile, the carbonyl absorption band of compound **3b** appeared at 1685 cm^{1}, and the absorption of the hydroxyl group occurred at 3460–3257 cm^{-1}. The representative ^{1}H NMR spectrum of compound **6a** showed singlet signals at 10.69 and 11.36 ppm, assigned to the OH and NH protons, respectively.

The multicomponent reaction of **3a** or **3b**, malononitrile (**8**), and the aromatic aldehyde derivatives (**7a–d**) in refluxing ethanol, and in the presence of the catalytic amount of piperidine, afforded the corresponding azo dyes, containing chromene moieties **9a–e** (Scheme 2).

The sequence of the reaction was initiated by the condensation of malononitrile (**8**) and the aldehyde derivatives (**7a–d**) to generate arylidinemalononitrile, which is manipulated as intermediates. These intermediates have been captured by the aromatic (CH-) of 2-naphthol to give a non-isolable product. The intermolecular Michael type addition of the latter intermediate furnished the respective benzo[*g*]chromene-3-carbonitriles (**9a–e**) as the end product. The characterization of the isolated products has been performed, using the spectroscopic techniques (FTIR, ^{1}H-NMR, and ^{13}C-NMR). For example, the IR spectrum of compound **9e** revealed stretching vibration bands at 2195 and 1450 cm^{-1} for the (CN) and the (N = N), respectively. In addition, a pair of bands at 3460 and 3420 cm^{-1} was assigned to the (NH_2) group. The ^{1}H NMR of **9e** exhibited singlet signals at 5.74 and 5.97 ppm for the CH-pyran at position-4 and the NH_2-protons, respectively (Widelski et al. 2009). Also, the ^{13}C NMR spectrum revealed a characteristic signal at 43.57 ppm, which was assigned to the C-4 of the pyran ring (Widelski et al. 2009).

To explore the scope of the multicomponent reactions, we extended the procedure to various arylazo dyes. Thus, refluxing a mixture of [5-substituted-2-((2,4-dihydroxyphenyl) azo) phenyl] [phenyl]methanone (**6a**, **b**), malononitrile (**8**), and arylaldehydes (**7a–d**) under similar conditions led to the formation of the corresponding 2-amino-6-[(2-benzoyl-4-substitutedphenyl) azo]-7-hydroxy-4-aryl-4*H*-chromene-3- carbonitriles (**10a–e**) (Scheme 3).

The elucidation of the structure of the isolated products was confirmed by the spectral data. The IR spectra showed stretching vibration bands at 3465–3460, 2220–2190, and

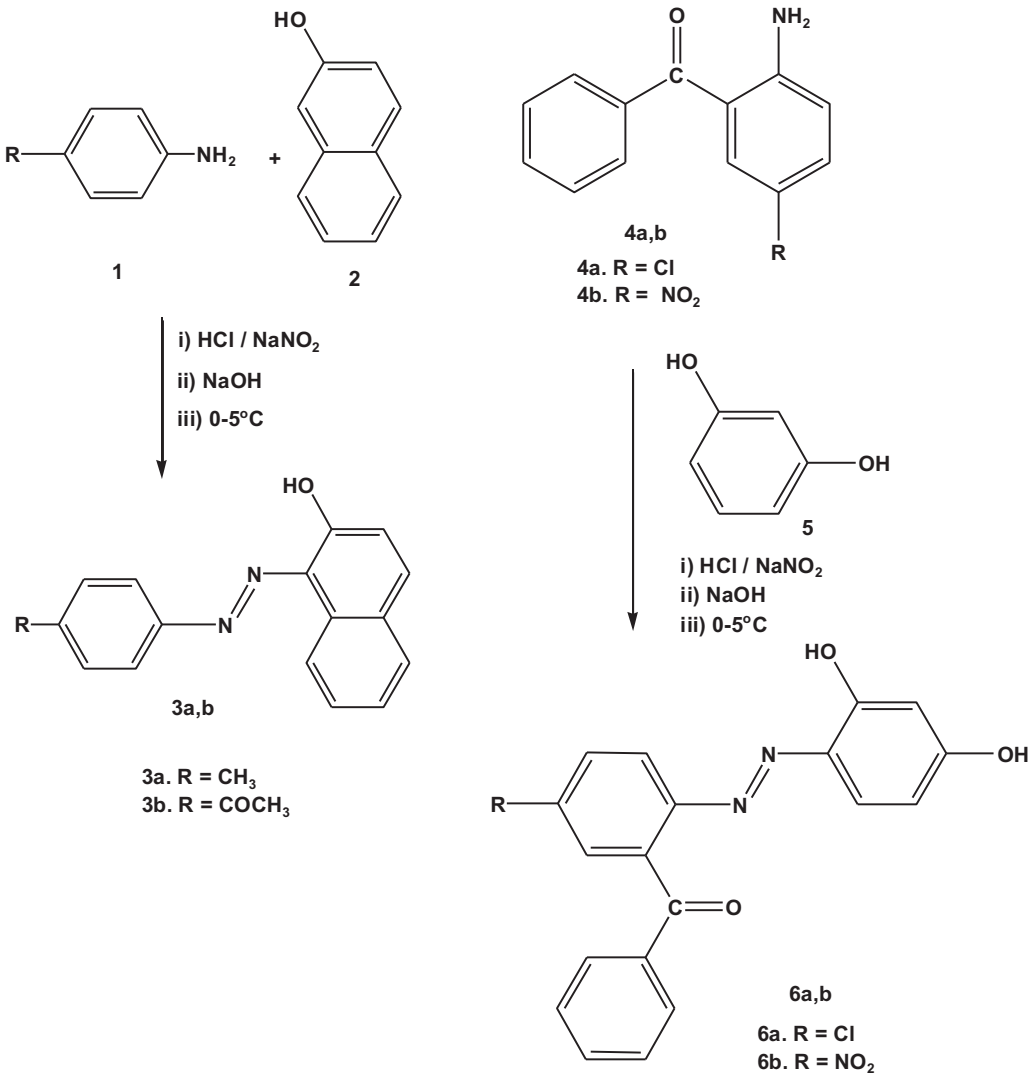

Scheme 1 The synthesis of azo chromophores **3a, b** and **6a**, **b**

1450 cm^{-1} for the (OH), (CN), and (N = N), respectively. In addition, a pair of bands at 3455–3450 and 3260–3220 cm^{-1} were ascribed to the (NH_2) group. The ^1H NMR exhibited singlet signals at 4.65–4.70, 8.54–9.88, and 11.33–11.59 ppm for the CH-pyran at the 4 position, the (OH) group, and the NH-hydrazone, respectively, while the broad signal at 6.88–7.05 ppm was assigned to the amino protons. Furthermore, the ^{13}C NMR spectra of compounds **10a–e** revealed characteristic signals between 35.63-36.85 ppm, which corresponds to the C-4 of pyran ring (Widelski et al. 2009).

UV-Vis Study

The UV-Vis analysis of the azo dyes **3a**, **b** and **6a**, **b** and arylazo chromene **10a–e** compounds revealed that the incorporation of the chromene moieties into the azo chromophores has no effect on their wavelength values. This behavior is due to the non-conjugated system of the chromene motifs and is consistent with our previous report (Afifi et al. 2017). Table 1 shows the UV-Vis of compounds **3a**, **b**, **6a**, **b** and the isolated products **10a–d** as representative examples of the target molecules. Moreover, the structures of the azo dyes **3a**, **b** and **6a**, **b** and the isolated products **10a–d** could have more than one tautomeric form, namely as hydroxyl-azo (**A**) or keto-hydrazone (**B**) (Fig. 2).

The electronic absorption spectral data of the investigated azo dyes (**3a**, **b** and **6a**, **b**) and the arylazo chromenes **10a–d** can be used to differentiate between the hydroxyl-azo (**A**) and the keto-hydrazone one (**B**), which exhibited a split peak for the latter form. As shown in Table 1, compounds **3a**, **10a**, and **10c** exhibited two absorption bands at (354–398 and 404–444 nm) in the DMF solution while **3b**, **6a**, **6b**, **10b**, and **10d** gave a single absorption peak at

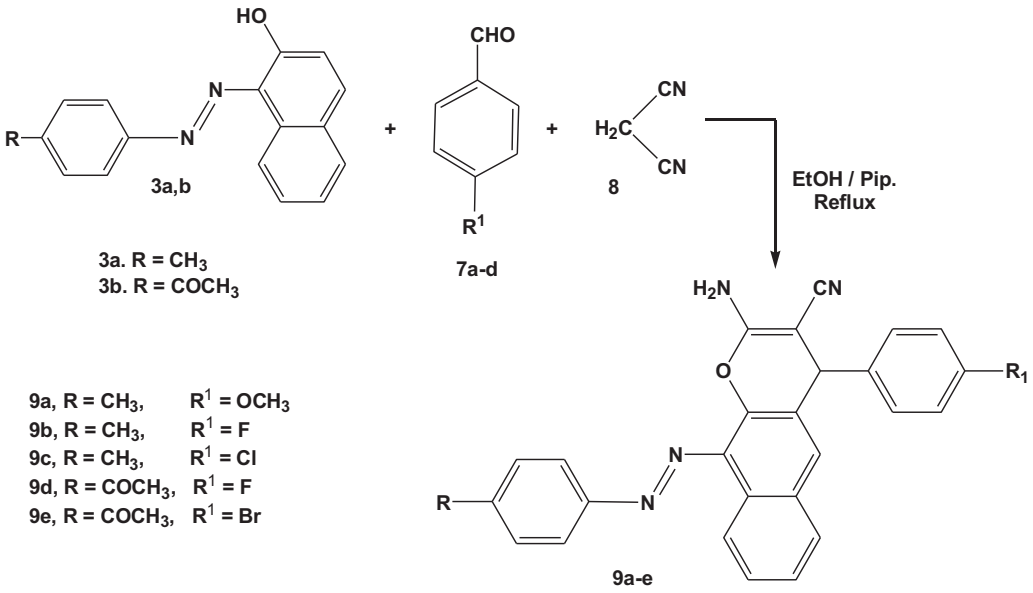

Scheme 2 Synthesis of benzo[*g*]chromenes containing azo chromophore moieties **9a–e**

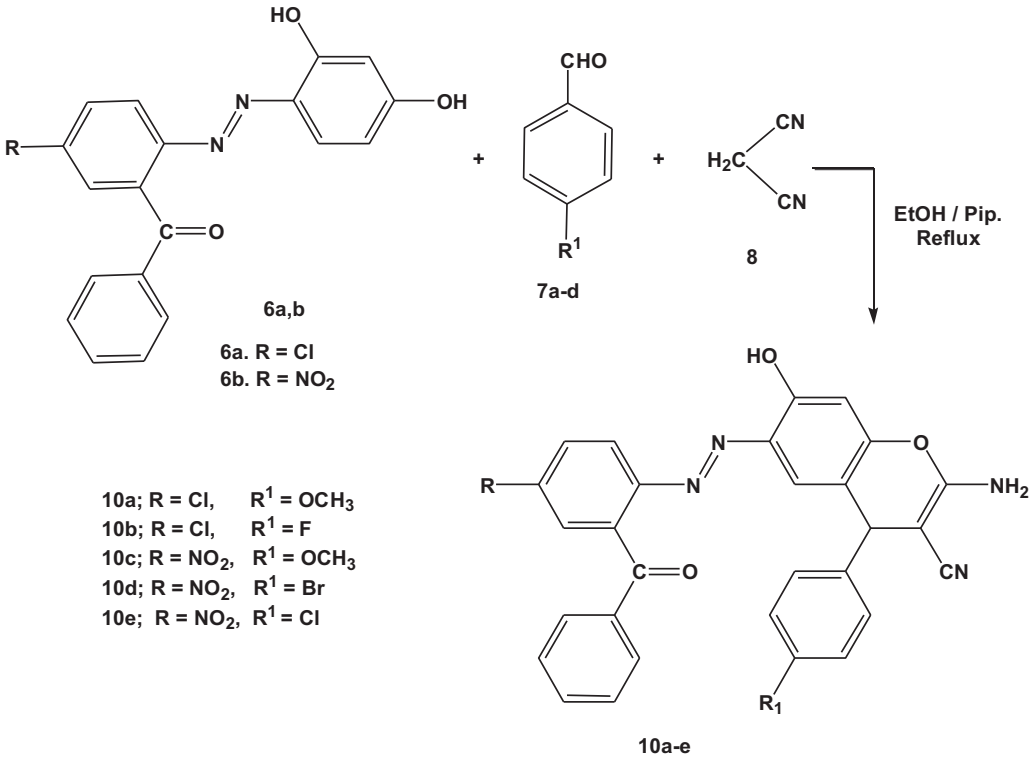

Scheme 3 Synthesis of azo chromene derivatives **10a–e**

(405–444 nm). The probable reason for this behavior is that the dyes **3a**, **10a**, and **10c** are present predominantly in a mixture of the hydroxyl-azo (**A**) and keto-hydrazone (**B**) forms while the other dyes **3b**, **6a**, **6b**, **10b**, and **10d** are presented in a single tautomeric form [keto-hydrazone (**B**)] (Wainwright 2008). This behavior was in a good agreement with the explanation for the ^{1}H NMR spectra for these dyes due to the presence of the NH signal in the regions of 11.33–16.15 ppm. A bathochromic shift was also observed in the DMF solution for the azo dye **3b** ($\lambda_{max} = 440$ nm) as compared to **3a** ($\lambda_{max} = 409$ nm), due to the effect of the electron withdrawing character of the acetyl group.

Table 1 UV absorption bands of compounds **3a, b**, **6a, b**, and **10a–d**

Compound No.	Substituents	λ_{max} (nm)	Absorbance
3a	$R = CH_3$	398, 409	1.33, 1.32
3b	$R = COCH_3$	440	1.5
6a	$X = Cl$	405	1.34
6b	$X = NO_2$	407	1.36
10a	$X = Cl$; $Ar = 4\text{-}CH_3OC_6H_4$	362, 404	1.62, 1.49
10b	$X = Cl$; $Ar = 4\text{-}FC_6H_4$	442	1.4
10c	$X = NO_2$; $Ar = 4\text{-}CH_3OC_6H_4$	354, 444	1.48, 0.67
10d	$X = NO_2$; $Ar = 4\text{-}ClC_6H_4$	444	1.55

ADMET predictions

In the current biomedical framework, the in-silico computer-aided drug designing (CADD) concept expedites virtual screenings from a vast quantity of compound libraries into miniature clusters of projected bioactive candidates, thus, optimizing the ADMET (absorption, distribution, metabolism, excretion, and toxicity) outline and bypassing the hurdles affiliated to safety. The prediction of the Blood–Brain Barrier (BBB) penetration plays a key role in the pharmaceutical sphere by determining whether the selected drug candidates would be able to pass across the blood – brain barrier or not. Compounds, which are Central Nervous System (CNS) active, are proficient in passing across the BBB (Ma et al. 2005). The venture of a drug's action in terms of its efficacy and disposition is governed by its binding to the plasma proteins (PPB), therefore, making the PPB% a major pharmacokinetic factor (Mannhold et al. 2008). The forecasting of the human intestinal absorption (HIA%) is equally appraised as a critical feature in the drug development phase. The ratio of excretion/cumulative excretion in urine, bile, and feces is applied to gauge the sum of absorption and bioavailability as HIA% (Zhao et al. 2010). In order to predict the oral absorption of drugs, models viz., the Madin–Darby canine kidney (MDCK) and Caco-2 cells are judged to be well-grounded in-vitro models (Hou et al. 2004; Irvine et al. 1999). The Ames test is a straight forward method to foretell the mutagenicity and carcinogenicity of the targeted compound (Bruce et al. 1973).

PreADMET was used to forecast the in-vivo ADMET properties of all the synthesized compounds i.e. information of rates for the BBB penetration, PPB%, HIA%, Caco-2, MDCK cell permeability and P-glycoprotein substrate inhibition, Table 2. All the investigated compounds can be classified as CNS candidates specially the compounds **3a** and **6a**, with highest absorption to CNS. All the standard drugs except vinblastine were predicted as non-CNS candidates. All the tested compounds can be categorized as well absorbed compounds as they displayed good human intestinal absorption with HIA% from 87.39%–100% including the standard drugs namely ampicillin and vinblastine with predicted HIA% of 81.48 and 96.06 respectively. The tested synthesized compounds also appeared as potent plasma protein binding candidates with PPB more than 90%. The predictions of PPB in standard drugs revealed to be lower ranging from 31.16%–71.67%. Compounds **4b** and **6b** likewise ampicillin and gentamicin exhibited low Caco-2 cell permeability while all the other compounds and standard drugs showed moderate Caco-2 cell permeability, ranging from 11.00% to 39.36% with highest predicted Caco-2 permeability of 39.36% for the standard drug, vinblastine. Most of the compounds along with the standard drugs were predicted as low permeable compounds for the MDCK cells (0.03%–21.12%). **3a**, **4a**, and **4b** have displayed moderate MDCK cell permeability (29.92%–76.92%). All the predicted compounds are P-gp inhibitors except for **4a**. Amphotericin B and vinblastine were forecasted as P-gp inhibitors while rest of the drugs were predicted as non-inhibitors. The toxicity in terms of mutagenicity (Ames Test) and carcinogenicity (mouse and rat) for the tested compounds/drugs is reported in Table 3. All the focused compounds and some standard drugs are predicted as mutagenic by the Ames test except for **10a**, **10d**, **10e**, Amphotericin B, vinblastine and doxorubicin. The prediction of carcinogenicity revealed that most of the tested compounds and all the predicted standard drugs except amphotericin B, possess carcinogenic activity in mouse. The forecast of rat carcinogenicity discloses that most of the tested compounds and standard drugs are carcinogenic in nature.

In-silico molecular docking studies

While designing a candidate drug, interaction between drug candidates and the targeted receptor is mostly understood by employing the molecular docking studies. This not only predicts the activity but also foretells the affinity of the tested drug candidates on the chosen receptor. Enzymes, which are associated with the biosynthetic procedure of the microbes' cell wall, are estimated to be the supreme targets for docking while designing novel compounds as antimicrobial drug candidates. The enzyme glucosamine-6-phosphate synthase (GlmS, GlcN-6-P synthase, L-glutamine: D-fructose-6P amido-transferase, EC 2.6.1.16) is materialized to be an attractive target for performing docking studies while designing both antibacterial and antifungal drug candidates (Chmara et al. 1984). This particular enzyme is involved in the genesis of the chief building block, namely *N*-acetyl Glucosamine (the core amino sugar) of the fungal and bacterial cell wall (Marshall

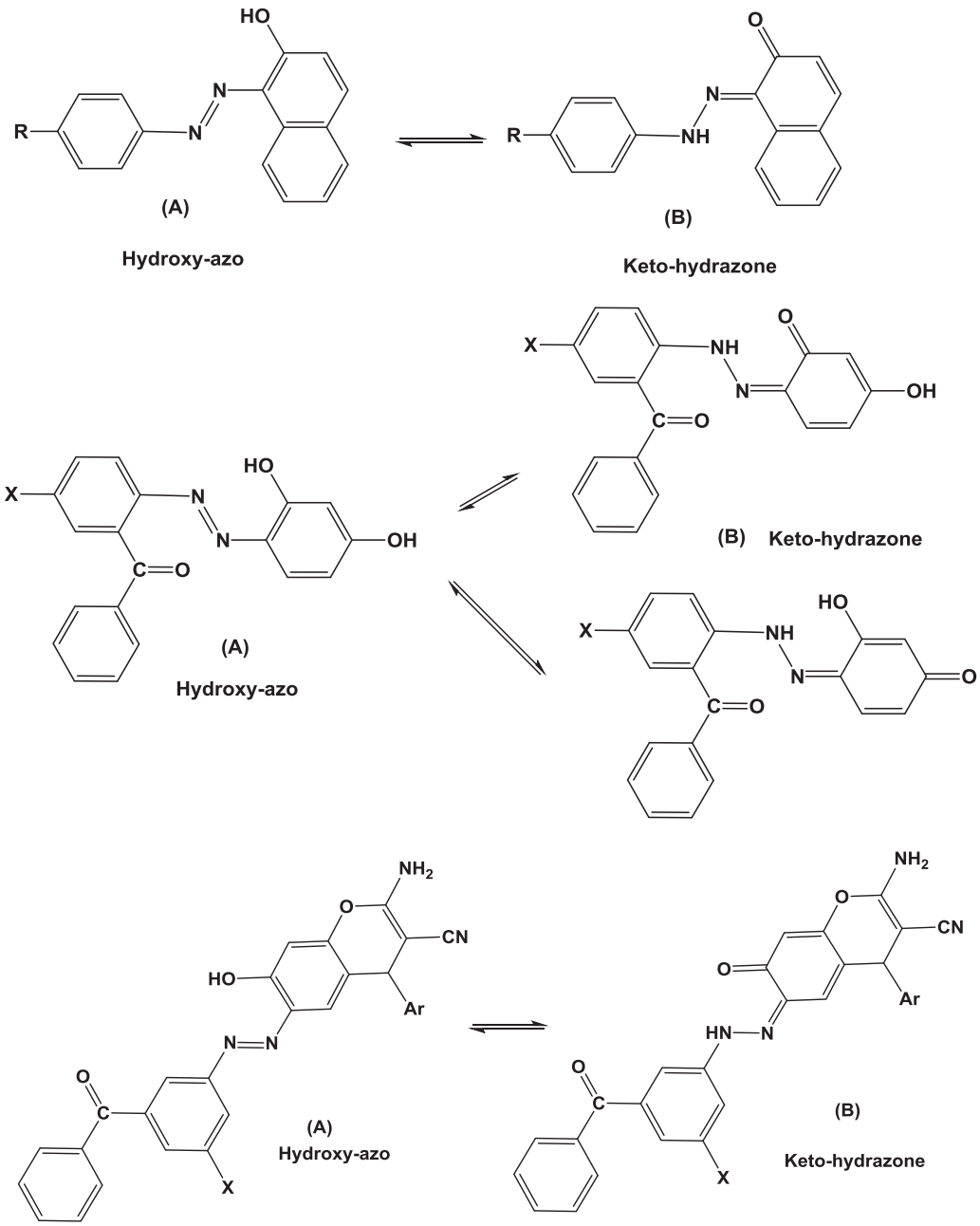

Fig. 2 Tautomeric forms of the azo dyes **3a, b** and **6a**, **b** and the arylazo chromenes **10a–d**

et al. 2003; Lather et al. 2018). The molecular docking was considered to study the binding interactions of the synthesized compounds with the target protein GlcN-6-P synthase (PDB ID: 2VF5).

Phosphoinositide 3-kinases (PI3Ks) is a member of the lipid kinases family and plays a crucial role in boosting the survival and cellular growth of several types of cancer. In cancer cells, the PI3Ks are the mandatory regulators of apoptosis. The PI3Ks catalyzes the phosphorylation of phosphatidylinositol of the inositol ring at the 3′-OH position, procuring the secondary messenger lipid, namely phosphatidylinositol-3,4,5-trisphosphate. This trisphosphate activates the serine/threonine kinase AKT, which in turn regulates several signaling pathways, thus, governing the survival of cells, the apoptosis process, the proliferation of cells, and the motility (Engelman 2009; Zhao and Vogt 2008). PI3Ks are categorized into three classes on basis of their structural traits and substrate specificity. Class I PI3Ks are the most assessed class of PI3Ks and it is grouped into 4 isoforms: p110α, p110β, p110δ, and p110γ. The PI3KCA gene, encoding p110α, is the most routinely mutated gene in human tumors, thus, inculcating to be the most striking

Table 2 In-silico ADME properties of the selected compounds/some standard drugs

Compound No.	BBB[a]	PPB[b]	HIA[c]	Caco-2[d]	MDCK[e]	P-gp[f]
3a	2.82	92.41	96.05	29.50	76.92	Inhibitor
3b	0.97	99.25	97.07	22.04	0.10	Inhibitor
9a	0.20	90.47	97.00	29.58	4.21	Inhibitor
9b	0.25	99.66	97.03	24.39	8.49	Inhibitor
9c	0.24	100	97.36	22.25	21.12	Inhibitor
9d	0.97	99.26	97.07	22.04	0.10	Inhibitor
9e	0.61	100	97.35	21.16	0.03	Inhibitor
4a	0.91	87.39	96.18	11.00	29.92	Non-inhibitor
4b	0.85	88.76	93.54	0.83	48.16	Inhibitor
6a	2.55	97.59	94.74	19.23	0.16	Inhibitor
6b	0.19	100	90.03	6.99	0.08	Inhibitor
10a	0.10	100	96.23	20.42	0.04	Inhibitor
10b	0.17	100	96.10	20.33	0.04	Inhibitor
10c	0.57	100	93.48	15.23	0.04	Inhibitor
10d	0.94	100	97.68	18.74	0.04	Inhibitor
10e	0.93	100	96.93	18.68	0.04	Inhibitor
Ampicillin	0.06	36.16	81.48	0.63	0.94	Non-inhibitor
Gentamicin	0.03	46.93	5.28	4.47	0.47	Non-inhibitor
Amphotericin B	0.03	39.01	4.68	14.14	0.04	Inhibitor
Vinblastine	0.87	71.67	96.06	39.36	0.04	Inhibitor
Colchicine	0.02	65.42	96.90	37.45	119.16	Non-inhibitor
Doxorubicin	0.04	31.16	56.84	17.73	1.02	Non-inhibitor

[a]Blood–brain barrier penetration, [b]Plasma protein binding, [c]Human intestinal absorption, [d]Caco-2 cell permeability, [e]MDCK cell permeability, [f]P-glycoprotein substrate

target for tumor therapy (Mukohara 2015; Liu et al. 2014; Yuan and Cantley 2008). Molecular docking screenings were performed to gain a better understanding of the binding mode of the synthesized compounds with the PI3K p110α domain (PDB ID: 2RD0).

In order to establish the best in-silico conformation, the molecular docking screenings of the newly synthesized compounds on the Glucosamine-6-phosphate of the GlcN-6-P synthase and the PI3K as the target proteins was executed. To please this motive, a Lamarckian genetic algorithm docking program, AutoDock 4.0, was employed. All the synthesized compounds were docked on these two target receptors. The docking of some selected ligands (with the highest docking score among the tested compounds) is shown in Fig. 3a, b. The minimum binding energy of all the docked compounds on the respective receptors is documented in Table 4. The ligands (synthesized compounds and the standard drugs) exhibited good in-silico docking scores towards the target receptors viz., the GlcN-6-P synthase, and PIK3, ranging from −8.7 to −6.37 and −10.2 to −7.0 Kcal/mol, respectively. Compound **9e** possess the highest docking score of −8.7 towards the GlcN-6-P synthase, and compounds **4a** and **6a** displayed the highest docking score of −9.8 towards PIK3.

Biological study

Antimicrobial activity

The compounds **3a**, **b**; **4a**, **b**; **6a**, **b**; **9a–e** and **10a–e** were screened for their antimicrobial activity against two gram positive bacteria [S.P (***S****treptococcus* ***p****neumoniae*) and B.S (*Bacillus* ***s****ubtilis*)], two gram negative bacteria [P.A (*Pseudomonas* ***a****eruginosa*) and E.C (*Escherichia* ***c****oli*)], and four Fungi [A.F (*Aspergillus fumigatus*), S.R (*Syncephalastrum racemosum*), G.C (*Geotricum candidum*), and C.A (*Candida* ***a****lbicans*)], using the diffusion agar technique (Widelski et al. 2009) at different concentrations. Ampicillin, Gentamicin, and Amphotericin B were used as control drugs (Yadav et al. 2007). The observed inhibition zone (IZ) is given in Table 5 and presented in Figs 4 and 5 while Table 6 illustrates the MIC values of the most active molecules.

Evidently, some of the investigated compounds exhibited moderate to good activity against gram positive bacteria (*Streptococcus pneumonia*, *Bacillis subtilis*) and gram negative bacteria (Escherichia *coli*). However, compounds **3b**, **9a**, **9d**, **9e**, and **4b** didn't demonstrate activity against the gram negative bacteria (*Pseudomonas aeruginosan*).

Table 3 In-silico toxicity prediction of the selected compounds/some standard drugs

Compound No.	Ames Test Mutagenicity	Mouse Carcinogenicity	Rat Carcinogenicity
3a	Mutagenic	Negative	Negative
3b	Mutagenic	Negative	Negative
9a	Mutagenic	Positive	Positive
9b	Mutagenic	Positive	Negative
9c	Mutagenic	Positive	Negative
9d	Mutagenic	Negative	Positive
9e	Mutagenic	Negative	Negative
4a	Mutagenic	Positive	Negative
4b	Mutagenic	Negative	Positive
6a	Mutagenic	Negative	Negative
6b	Mutagenic	Negative	Positive
10a	Non-Mutagenic	Negative	Negative
10b	Mutagenic	Negative	Negative
10c	Mutagenic	Negative	Positive
10d	Non-Mutagenic	Negative	Negative
10e	Non-Mutagenic	Negative	Negative
Ampicillin	Mutagenic	Negative	Negative
Gentamicin	Mutagenic	Negative	Negative
Amphotericin B	Non-Mutagenic	Positive	Positive
Vinblastine	Non-Mutagenic	Negative	Positive
Colchicine	Mutagenic	Negative	Positive
Doxorubicin	Non-Mutagenic	Negative	Negative

Among the azo dye derivatives, **6a** displayed good activity against (*Streptococcus pneumonia*) and (*Bacillis subtilis*) with respect to the standard drug Ampicillin as shown in Table 5. In addition, **3a** and **9b** showed higher activity against (*Pseudomonas aeruginosa*) and (*Escherichia coli*) in comparison to the reference drug Gentamicin, Table 5. Moreover, the obtained results imply that compounds **3a**, **9b**, **9e**; **6a** and **10b** could be attractive new antibacterial drugs.

As shown in (Table 5) and (Fig. 6), the antifungal performance of the target compounds, which displays moderate to good activity against the studied fungi (*Aspergillus fumigates*, *Syncephalastrum racemosum*, *Geotricum candidum* and *Candida albicans*). Based on the obtained data, compounds **3a**, **9c**, **9d**, **4a**, **4b**, **6a**, **6b**, **10a**, **10d**, and **10e** did not exhibit any activity against (*Syncephalastrum racemosum*). However, **3b**, **6a**, **6b**, and **10b** derivatives portrayed very good antifungal activity against most of the fungi as compared to the reference drug Amphotericin-B.

Cytotoxic screening

The in-vitro cytotoxic activity of the studied molecules was performed by the MTT assay (Alley et al. 1988) against three human carcinoma cell lines: human colon carcinoma (HCT-116), human hepatocellular carcinoma (HEPG-2), and human breast adenocarcinoma (MCF-7). Doxorubicin, Vinblastine, and Colchicine were used as positive controls. The inhibitory effects of compounds **3a**, **b**, **4a**, **b**, **6a**, **b**, **9a–e**, and **10a–e** on the growth of the three cell lines are presented in Table 7.

As can be seen from Table 7 and Fig. 7, the values of compounds **3b**, **4a**, **6a**, **9d** and **9e** from the investigated compounds in comparison to Colchicine as reference drug exhibited good IC_{50}s, ranging from 5.4 to 19.2 µM, against the HCT-116 cell line. While compounds **3a**, **3b**, **4a**, **6a**, **6b**, **9d** and **9e** displayed inhibitory effects against the MCF-7 cell line with IC_{50} (8.6–44.3 µM), excluding **9a** and **9b**, which accounts for the same value of Colchicine as standard drug. Moreover, the compounds **3b**, **6a**, **9d** and **9e** showed slightly high activity in the case of the HepG-2 cell line by an IC_{50} range of (10.6 to 15.0 µM). All the investigated compounds displayed less activity against the three cancer cell lines as compared to both Vinblastine and Doxorubicin reference drugs.

Conclusion

A new series of azo dyes, containing chromene moieties, has been synthesized, using the multicomponent reaction (MCRs) strategy containing azo dye, malononitrile, and the corresponding aldehydes. The structure identity of the desired compounds was confirmed, using the spectroscopic techniques. These molecules have been employed for several theoretical studies in order to predict their performance as a new drug system. ADMET properties were predicted in order to gauge the pharmacokinetic and pharmacodynamic features of the synthesised compounds. As per predictive results, the analyzed compounds can be classified as CNS and skillfully absorbed candidates as compared to the predicted standard drugs, as the synthesized compounds flaunted good BBB permeation (≥0.1) and HIA% (87.39%–100%) along with PPB more than 90%. Most of the predicted compounds emerged as P-gp inhibitors along with Amphotericin B and vinblastine. The predicted compounds possess low to moderate Caco-2 and MDCK cells permeability with the highest predicted Caco-2 permeability for vinblastine (39.36%). The toxicity prediction reveals that most of the compounds are mutagenic in nature when compared with the predicted non-mutagenic nature of some of the standard drugs. Most the tested compounds and standard drugs were forecasted to be carcinogenic both in

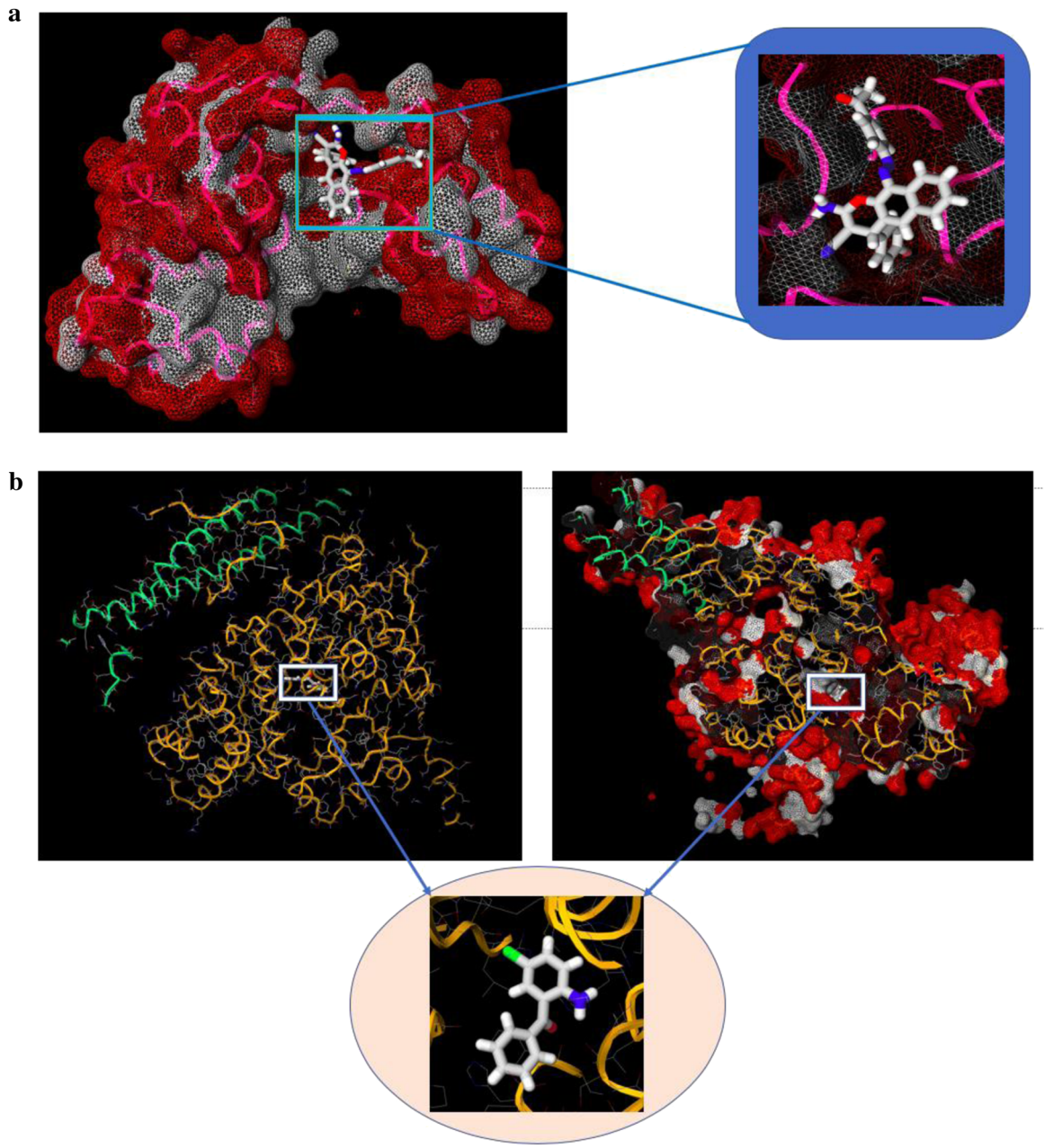

Fig. 3 **a** Docking of compound **9e** into active site of glucosamine-6-phosphate (GlcN-6-P) synthase (PDB ID: 2VF5). **b** Docking of compound **4a** into active site of Phosphoinositide 3-kinases (PI3K, PDB ID: 2RD0)

rat and mouse except amphotericin B. In-silico molecular docking study unveiled the interaction between the synthesized ligands and the targeted protein receptor to be favorable with good docking scores. The highest docking score was obtained by compound **9d** i.e −8.7 Kcal/mol towards the GlcN-6-P synthase, and compounds **4a** and **6a** i.e −9.8 Kcal/mol towards PIK3.

In order to endorse these in-silico results, the new compounds were then screened for their in-vitro antimicrobial and antitumor behaviour, sequentially, investigate their potential as new drug candidates. The antibacterial study stated that compounds **3a**, **6a**, **6b**, **9e**, and **10b** have the most antibacterial effect while **3b**, **6a**, **6b**, and **10b** derivatives displayed very good antifungal activity against most of the tested fungi. The in-vitro results were validated as these compounds emerged as promising candidates in the molecular docking studies with energetically favorable binding poses and good docking score as compared to other compounds which are neither promising candidates in in-silico nor in in-vitro *studies*. Meanwhile, the in-vitro anticancer examination showed that most of the target molecules displayed unexpected comparable cytotoxicity to

Table 4 Docking scores as minimum binding energy (Kcal/mol) of the synthesized compounds/standard drugs on the target receptors i.e GlcN-6-P synthase and PIK3 respectively

Compound no.	GlcN-6-P synthase	PIK3
3a	−7.3	−8.5
3b	−7.5	−9.7
9a	−8.1	−8.3
9b	−8.2	−8.1
9c	−8.5	−8.4
9d	−8.6	−9.6
9e	−8.7	−9.6
4a	−6.6	−9.8
4b	−7.1	−8.4
6a	−8.1	−9.8
6b	−8.4	−8.4
10a	−7.5	−7.6
10b	−8.1	−7.6
10c	−5.7	−7.0
10d	−6.4	−7.4
10e	−6.5	−7.8
Ampicillin	−7.8	–
Gentamicin	−7.4	–
Amphotericin B	−8.1	–
Vinblastine	–	−9.5
Colchicine	–	−9.3
Doxorubicin	–	−10.2

the reference drug, in particular, compounds **3b**, **4a**, **6a**, **9e** and **9d** which demonstrated good IC_{50} values against the HCT-116 cell line, as compared to Colchicine. While, compounds **3a**, **3b**, **4a** and **6a** exhibited excellent IC_{50} values against the MCF-7, as compared to Colchicine. These results were found to be consistent with the in-silico molecular docking studies as these compounds **3b**, **4a**, **6a**, and **9d** had shown the highest binding energy toward the target protein PIK3 ranging from −9.8 to −9.6 kJ mol^{-1} and have good affinity toward the protein. Thus, they may be considered as good inhibitors of PIK3 by in-silico studies which was supported by good in-vitro anticancer results. This alliance between in-silico and in-vitro studies may facilitate structural based design of more potent and selective compounds in the future.

Experimental section

Materials & instrumentation

All the melting points are measured by a MEL-TEMP Electrothermal Melting point apparatus and were uncorrected. The IR absorption spectra were recorded by a Shimadzu IR – 8400S, using the KBr pellets (ν in cm^{-1}). The NMR spectra were recorded on a Bruker Avance 400 MHz, spectrometer, using the TMS as an internal standard and the $CDCl_3$ (DMSO) as solvents, [Chemical shifts in δ (ppm)]. The MS were measured on a Shimadzu GC/MS-QP5050A spectrometer. The UV-Vis spectra were recorded on a Jasco UV-Vis spectrophotometer double-beam spectrophotometer (range 350 to 700 nm) with the scan speed at 200 nm min^{-1}, using a 1.0 cm quartz cell. A cell containing the pure solvent was used as reference. All

Table 5 Mean zone of inhibition in mm produced on a range of environmental clinically pathogenic microorganisms using (5 mg/mL) concentration of tested samples

Compounds	Tested microorganisms							
	Gm +ve		Gm −ve		Fungi			
	S.P	B.S	P.A	E.C	A.F	S.R	G.C	C.A
3a	16.4	17.3	17.5	19.3	16.2	NA	17.6	17.2
3b	16.2	18.1	NA	15.6	19.3	17.2	21.3	18.3
9a	17.5	19.3	NA	16.6	18.5	17.8	19.4	17.5
9b	18.6	18.7	19.2	17.6	17.7	18.3	19.7	18.5
9c	17.6	18.2	16.5	17.8	18.6	NA	18.8	19.3
9d	18.2	17.5	NA	18.2	17.5	NA	19.2	18.8
9e	18.5	19.2	NA	18.2	17.8	19.6	19.6	18.5
4a	17.3	16.8	16.8	17.5	16.5	NA	17.4	16.8
4b	16.8	17.4	NA	17.2	17.6	NA	16.8	17.6
6a	20.2	23.8	16.3	17.5	19.8	NA	22.3	21.1
6b	19.2	20.1	17.9	16.2	18.2	NA	21.4	20.6
10a	16.7	17.8	14.6	16.5	15.7	NA	16.1	15.2
10b	17.8	18.2	16.5	15.4	19.2	16.7	20.5	19.8
10c	15.9	16.1	15.8	15.2	17.8	16.3	18.7	19.6
10d	17.5	16.8	16.2	15.3	16.5	NA	17.9	18.5
10e	18.1	17.7	16.5	16.2	17.3	NA	17.2	18.6
Ampicillin	23.8	32.4	–	–	–	–	–	–
Gentamicin	–	–	17.3	19.9	–	–	–	–
Amphotericin B	–	–	–	–	23.7	19.7	28.7	25.4

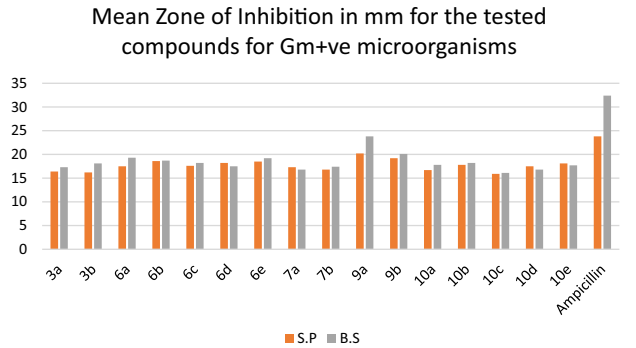

Fig. 4 Gm +ve microorganism antibacterial activity of the investigated compounds

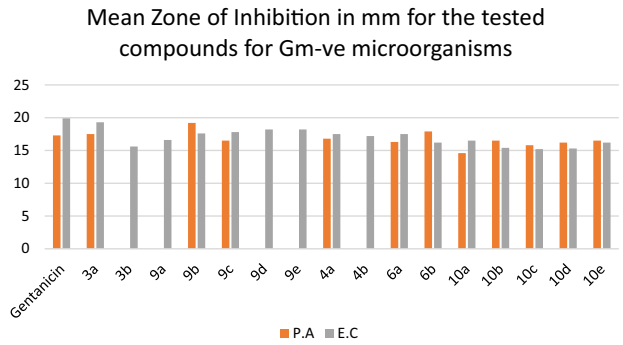

Fig. 5 Gm −ve microorganism antibacterial activity of the investigated compounds

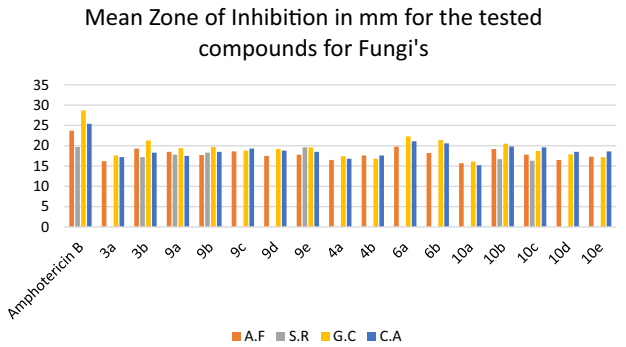

Fig. 6 Antifungal activity of the investigated compounds

Table 6 MIC (μg/mL) of tested samples against tested microorganisms

Compounds	Tested microorganisms							
	Gm +ve		Gm –ve		Fungi			
	S.P	*B.S*	*P.A*	*E.C*	*A.F*	*S.R*	*G.C*	*C.A*
3b	7.81	3.9	NA	31.25	3.9	7.81	1.95	3.9
9a	7.81	7.81	NA	31.25	3.9	7.81	3.9	31.25
9b	7.81	3.9	1.95	7.81	7.81	3.9	1.95	7.81
9c	31.25	7.81	31.25	7.81	3.9	NA	3.9	1.95
9d	7.81	7.81	NA	7.81	7.81	NA	1.95	3.9
9e	7.81	3.9	NA	3.9	7.81	1.95	1.95	7.81
4a	7.81	31.25	31.25	7.81	31.25	NA	7.81	31.25
6a	3.9	1.95	31.25	7.81	3.9	NA	1.95	3.9
6b	7.81	3.9	31.25	31.25	7.81	NA	3.9	1.95
10a	7.81	7.81	31.25	15.63	31.25	NA	15.63	31.25
10b	7.81	3.9	7.81	31.25	3.9	16.7	1.95	3.9
10c	31.25	31.25	31.25	31.25	7.81	31.25	7.81	7.81
10d	15.63	31.25	31.25	31.25	15.63	NA	7.81	3.9
10e	7.81	7.81	31.25	31.25	15.63	NA	15.63	7.81
Ampicillin	0.98	0.24	–	–	–	–	–	–
Gentamicin	–	–	15.63	3.9	–	–	–	–
Amphotericin B	–	–	–	–	0.98	3.9	0.49	0.49

the measurements were made at room temperature. All reactions have been followed by the TLC. The biological evaluation of the products was carried out in the Medical Mycology Laboratory of the Regional Center for Mycology and Biotechnology of Al-Azhar University, Cairo, Egypt.

Chemistry

General procedure for the preparation of 1-arylazo-naphthalen-2-ol (3a,b) and [5-substituted-2-(2,4-dihydroxyphenylazo)-phenyl] [phenyl]methanone (6a, b)

Aniline derivatives **1a**, **b** or **4a**, **b** (10 mmol) were dissolved in a solution of hydrochloric acid and water. The mixture was stirred gently to ensure complete dissolution of aniline at 0–5 °C. Sodium nitrite (10 mmol), dissolved in water (10 mL), was used to diazotize the aniline derivatives at 0–5 °C. The nitrite solution was intermittently added to the amine solution with stirring, and the temperature was monitored to ensure that it did not exceed 5 °C. The diazonium salt solution was left in the freezing mixture and was stirred occasionally until the temperature came down to 0 °C for 2 hrs. The coupling component, 2-naphthol (**2**) or resorcinol (**5**) (10 mmol), was dissolved in a 10% sodium hydroxide solution and then cooled to 0 °C by adding ice. The previously prepared diazonium solution was added drop wise over 30 min with stirring. The mixture was stirred for a further 2 hrs. at 5 °C, and the pH of this solution was

Table 7 Inhibitory activity against HCT-116, MCF-7 and HepG-2 cell lines

Compounds	IC_{50} (μM)		
	HCT-116	MCF-7	HepG-2
3a	69.0	15.1	115.5
3b	14.9	9.5	10.6
9a	50.4	95.4	32.0
9b	50.4	96.9	26.7
9c	59.2	103.1	28.1
9d	19.2	44.3	14.2
9e	17.5	29.2	14.6
4a	11.4	12.1	43.1
4b	167.2	185.4	152.3
6a	5.4	8.6	15.0
6b	252.7	40.7	74.6
10a	374.3	159.4	307.3
10b	278.1	139.4	302.9
10c	253.9	170.8	144.3
10d	368.9	210.3	149.2
10e	298.9	207.6	126.6
Vinblastine	3.2	7.5	5.7
Colchicine	44.3	107.2	26.5
Doxorubicin	1.6	1.9	2.2

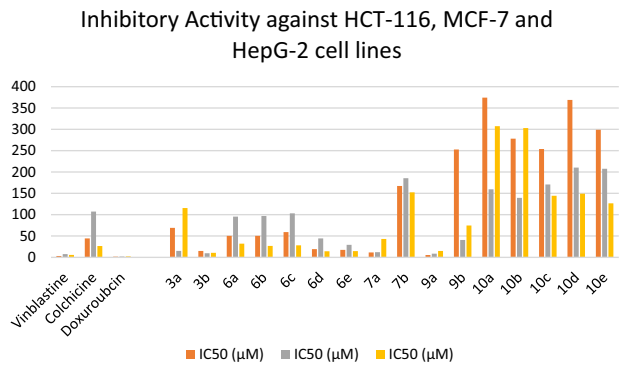

Fig. 7 Antitumor activity of the investigated compounds

adjusted to 4–5 by adding the hydrochloric acid slowly, followed by the filtration and washing until neutral and the drying and then crystallizing from ethanol afforded azo dyes **3a**, **b** or **6a**, **b**, respectively.

1-[(4-Methylphenyl)azo]naphthalene–2-ol (3a) Red solid (94%), m.p. 119 °C; IR (KBr) cm^{-1}: IR ν_{max} (cm^{-1}, KBr): 3436 (OH), 1446 (N = N); ^{1}H NMR ($CDCl_3$, ppm) δ: 2.41 (3H, s, CH_3), 6.92 (1H, d, $J = 9.2$ Hz, Ar–CH), 7.28 (2H, d, $J = 8$ Hz, Ar–CH), 7.39 (1H, t, Ar–CH), 7.55 (1H, t, Ar–CH), 7.62 (1H, d, $J = 8$ Hz, Ar–CH), 7.67 (2H, d, $J = 8$ Hz, Ar–CH), 7.72 (1H, d, $J = 9.2$ Hz, Ar–CH), 8.61 (1H, d, $J = 8$ Hz, Ar–CH), 16.15 (1H, s, NH hydrazo form); ^{13}C NMR ($CDCl_3$, ppm) δ: 21.30 (CH_3), 119.19, 121.64, 123.98, 125.32, 128.21, 128.50, 128.59, 129.91, 130.20, 133.71, 138.38, 138.85, 143.90 (Ar-C), 168.50 (C = O of hydrazo form).

1-[4-(2-Hydroxynaphthalene-1-ylazo)phenyl]ethanone (3b) Red solid (85%), m.p. 144 °C; IR (KBr) cm^{-1}: IR ν_{max} (cm^{-1}, KBr): 3257(OH), 1446 (N = N), 1685 (C = O); ^{1}H NMR ($CDCl_3$, ppm) δ: 2.61 (3H, s, $COCH_3$), 6.72 (1H, d, $J = 9.6$ Hz, Ar–CH), 7.40 (1H, t, $J = 6.8$ Hz, Ar–CH), 7.52-7.56 (2H, m, Ar–CH), 7.66–7.68 (3H, m, Ar–CH), 8.04 (2H, d, $J = 8.8$ Hz, Ar–CH), 8.43 (1H, d, $J = 8.4$ Hz, Ar–CH), 16.13 (1H, s, NH hydrazo form); ^{13}C NMR ($CDCl_3$, ppm) δ: 26.55 (CH_3), 116.91, 122.20, 126.17, 126.89, 128.35, 128.96, 129.49, 130.24, 131.21, 133.33, 134.29, 142.51, 146.76 (Ar-C); 178.44 (C = O of hydrazo form), 19676 ($COCH_3$).

[5-Chloro-2-(2,4-dihydroxyphenylazo)-phenyl] [phenyl] methanone (6a) Reddish orange solid (84%), m.p. 118 °C; IR (KBr) cm^{-1}: 3460, (OH), 1685 (CO), 1450 (N = N); ^{1}H NMR (DMSO-d_6, ppm) δ: 6.25 (1H, s, Ar–CH), 6.32-6.34 (1H, dd, Ar–CH), 7.14 (1H, d, Ar–CH), 7.50 (2H, t, Ar–CH), 7.63 (1H, t, Ar–CH), 7.69 (1H, d, Ar–CH), 7.71 (1H, d, Ar–CH), 7.72 (1H, s, Ar–CH), 7.78 (1H, d, Ar–CH), 8.02(1H, d, Ar–CH), 10.69 (1, s, OH), 11.36 (1H, s, NH hydrazo form); ^{13}C NMR (DMSO-d_6, ppm) δ: 103.29, 109.85, 120.61, 128.57, 128.66, 129.32, 129.67, 131.54, 132.87, 134,17, 134.71, 137.41, 137.79, 147.91, 157.09, 164.42 (Ar-C), 195.35 (C = O of carbonyl group).

[2-(2,4-Dihydroxyphenylazo)-5-nitrophenyl] [phenyl] methanone (6b) Red solid (76%), m.p. 154 °C; IR (KBr) cm^{-1}: 3460 (OH), 1685 (CO), 1450 (N = N); ^{1}H NMR (DMSO-d_6, ppm) δ: 6.28 (1H, s, Ar–CH), 6.35–6.50 (1H, dd, Ar–CH), 7.14 (1H, d, Ar–CH), 7.51 (2H, t, Ar–CH), 7.65 (1H, t, Ar–CH), 7.74 (1H, d, Ar–CH), 7.82 (1H, d, Ar–CH), 8.18 (1H, s, Ar–CH), 8.41 (1H, d, Ar–CH), 8.49 (1H, d, Ar–CH), 11.70 (1, s, OH), 13.78 (1H, s, NH hydrazo form).

General procedure for synthesis of 2-amino-4H-benzo[g] chromene-3-carbonitriles (9a–e) and 2-amino-4H-chromene-3-carbonitriles (10a–e)

A mixture of azodyes **3a**, **b** or **6a**, **b** (2.3 mmol), malononitrile (2.3 mmol), and aryl aldehyde (2.3 mmol) was dissolved in ethanol (10 mL) and few drops of pipredine were added. The reaction mixture was refluxed (4–6 h.). After the completion of the reaction (monitored by TLC), the mixture was cooled, filtered, and washed with ethanol and hexane to afford **9a–e** or **10a–e**, respectively.

2-Amino-4-(4-methoxyphenyl)-10-[(4-methylphenyl)azo]-*4H*-benzo[*g*]chromene- 3-carbonitrile (9a) Dark red solid (75%), m.p. 118 °C; IR (KBr) cm^{-1}: 3450, 3386 (NH_2), 2979, 2935, 2869 (CH), 2210 (CN), 1430 (N = N); ^1H NMR (DMSO-d_6, ppm) δ: 2.29 (3H, s, CH_3), 3.65 (3H, s, OCH_3), 4.95 (1H, s, CH pyran), 5.97 (2H, s, NH_2), 6.80-7.15 (4H, m, ArCH), 7.55–7.70 (4H, m, ArCH), 8.15–8.26 (2H, m, ArCH), 8.36 (1H, s, ArCH), 8.46 (2H, d, ArCH); ^{13}C NMR (DMSO-d_6, ppm) δ: 20.96 (CH_3), 40.57 (CH pyran), 52.8 (OCH_3), 60.83 (CN), 112.5, 115.5, 121.5, 122.6, 123.5, 125.8, 127.7, 129.2, 129.5, 130.08, 131.5, 132.8, 133.01, 134.6, 135.12, 136.9, 143.4, 148.6, 158.7, 177.7 (Ar-C). MS, m/z (%): 446 (M^+, 51.36) with a base peak at 259 (100).

2-Amino-4-(4-fluorophenyl)-10-[(4-methylphenyl)azo]-*4H*-benzo[*g*]chromene-3-carbonitrile (9b) Reddish-brown solid (70%), m.p. 126 °C; IR (KBr) cm^{-1}: 3266, 3258 (NH_2), 2979, 2935, 2869 (CH), 2200 (CN), 1430 (N = N); ^1H NMR (DMSO-d_6, ppm) δ: 2.31 (3H, s, CH_3), 5.45 (1H, s, CH pyran), 6.52 (2H, s, NH_2), 7.15–7.35 (4H, m, ArCH), 7.65–7.85 (4H, m, ArCH); 8.12–8.30 (2H, m, ArCH), 8.40 (1H, s, ArCH), 8.46 (2H, m, ArCH); ^{13}C NMR (DMSO-d_6, ppm) δ: 21.25 (CH_3), 39.95 (CH pyran), 60.83 (CN), 114.5, 118.5, 124.5, 126.6, 127.5, 128.8, 129.6, 129.9, 130.21, 131.87, 132.08, 133.5, 134.08, 135.8, 136.01, 138.6, 139.9, 145.4, 148.2, 161.7, 179.7 (Ar-C). MS, m/z (%): 434 (M^+, 45.62) with a base peak at 339 (100).

2-Amino-4-(4-chlorophenyl)-10-[(4-methylphenyl)azo]-*4H*-benzo[*g*]chromene-3-carbonitrile (9c) Dark red solid (72%), m.p. 118 °C; IR (KBr) cm^{-1}: 3450, 3278 (NH_2), 2979, 2935, 2869 (CH), 2220 (CN), 1435 (N = N); ^1H NMR (DMSO-d_6, ppm) δ: 2.29 (3H, s, CH_3), 5.45 (1H, s, CH pyran), 6.52 (2H, s, NH_2), 7.19–7.39 (4H, m, ArCH), 7.43–7.49 (4H, m, ArCH), 8.15–8.30 (2H, m, ArCH), 8.47 (1H, s, ArCH), 8.66 (2H, m, ArCH); ^{13}C NMR (DMSO-d_6, ppm) δ: 23.25 (CH_3), 40.95 (CH pyran), 62.73 (CN), 116.5, 117.5, 123.5, 125.6, 126.5, 127.9, 128.04, 129.6, 130.9, 131.25, 132.08, 133.5, 134.8, 135.69, 136.01, 137.6, 139.9, 145.4, 148.2, 160.7, 177.7 (Ar-C). MS, m/z (%): 450 (M^+, 32.46) with a base peak at 339 (100).

10-[(4-Acetylphenyl)azo]-2-amino-4-(4-fluorophenyl)-*4H*-benzo[*g*]chromene-3-carbonitrile (9d) Red solid (78%), m.p. 208 °C; IR (KBr) cm^{-1}: 3400, 3350 NH_2), 2979, 2935, 2869 (CH), 2210 (CN), 1445 (N = N); ^1H NMR (DMSO-d_6, ppm) δ: 2.67 (3H, s, $COCH_3$), 5.25 (1H, s, CH pyran), 6.59 (2H, s, NH_2), 7.15–7.35 (4H, m, ArCH), 7.65–7.85 (4H, m, ArCH), 8.19-8.35 (2H, m, ArCH), 8.40 (1H, s, ArCH), 8.46 (2H, m, ArCH); ^{13}C NMR (DMSO-d_6, ppm) δ: 26.96 ($COCH_3$), 41.57 (CH pyran), 60.83 (CN), 114.2, 116.1, 120.2, 121.3, 123.8, 127.4, 128.6, 129.9, 131.0, 132.08, 135.5, 138.0, 139.01, 140.5, 142.8, 146.6, 148.4, 157.6, 161.7, 178.6 (Ar-C), 197.39 (C = O). MS, m/z (%): 462 (M^+, 40.31) with a base peak at 367 (100).

10-[(4-Acetylphenyl)azo]-2-amino-4-(4-bromophenyl)-*4H*-benzo[*g*]chromene-3-carbonitrile (9e) Red solid (74%), m.p. 218 °C; IR (KBr) cm^{-1}: 3460, 3420 (NH_2), 2979, 2935, 2869 (CH), 2195 (CN), 1450 (N = N); ^1H NMR (DMSO-d_6, ppm) δ: 2.69 (3H, s, $COCH_3$), 5.74 (1H, s, CH pyran), 5.97 (2H, s, NH_2), 7.36 (2H, d, $J = 8.4$ Hz, ArCH), 7.56 (2H, d, $J = 8.4$ Hz, ArCH), 7.72-7.76 (2H, m, ArCH), 7.85 (1H, t, ArCH), 8.03 (1H, d, ArCH), 8.12 (1H, t, ArCH), 8.38 (2H, d, $J = 8.0$ Hz, ArCH), 8.82 (2H, d, J = 8.0 Hz, ArCH); ^{13}C NMR (DMSO-d_6, ppm) δ: 26.96 ($COCH_3$), 43.57 (CH pyran), 60.83 (CN), 102.1, 103.2, 121.3, 122.8, 127.4, 128.6, 129.9, 130.0, 130.08, 130.5, 131.0, 133.01, 135.5, 137.8, 138.6, 138.9, 143.4, 150.6, 151.7, 178.6, (Ar-C), 197.39 (C = O). MS, m/z (%): 522 (M^+, 51.36) with a base peak at 367 (100).

2-Amino-6-[(2-benzoyl-4-chlorophenyl)azo]-7-hydroxy-4-(4-methoxyphenyl)-*4H*- chromene-3-carbonitrile (10a) Reddish orange solid (84%), m.p. 250 °C; IR (KBr) cm^{-1}: 3460 (OH), 3450, 3220 (NH_2), 2220 (CN), 1685 (CO), 1450 (N = N); ^1H NMR (DMSO-d_6, ppm) δ: 3.85 (3H, s, OCH_3), 4.69 (1H, s, CH pyran), 6.65 (1H, s, Ar–CH), 6.88 (2H, s, NH_2), 6.95 (2H, d, ArCH), 7.05 (2H, t, Ar–CH), 7.15 (2H, d, Ar–CH), 7.45 (2H, t, Ar–CH), 7.65 (1H, t, Ar–CH), 7.69 (2H, d, Ar–CH), 8.19 (1H, s, Ar–CH), 9.81 (1, s, OH), 11.36 (1H, s, NH hydrazo form); ^{13}C NMR (DMSO-d_6, ppm) δ: 36.05 (CH pyran), 44.26 (OCH_3), 57.77 (CN), 108.9, 113.5, 114.2, 114.9, 114.22, 114.93. 122.43, 123.54, 124.23, 124.92, 126.11, 127.21, 128.65, 129.36, 129.67, 131.88, 132.39, 134.10, 136.51, 139.12, 147.83, 154.74, 159.95, 163.16, (Ar-C), 195.35 (C = O). MS, m/z (%): 536 (M^+, 35.64) with a base peak at 244 (100).

2-Amino-6-[(2-benzoyl-4-chlorophenyl)azo]-7-hydroxy-4-(4-fluorophenyl)-*4H*- chromene-3-carbonitrile (10b) Reddish orange solid (84%), m.p. 154 °C; IR (KBr) cm^{-1}: 3465 (OH), 3455, 3260 (NH_2), 2190 (CN), 1685 (CO), 1450 (N = N); ^1H NMR (DMSO-d_6, ppm) δ: 4.70 (1H, s, CH pyran), 6.15 (1H, s, ArCH), 6.25 (1H, s, ArCH), 6.33 (1H, t, ArCH), 6.60 (1H, d, $J = 9.2$ Hz, ArCH), 6.95 (2H, t, ArCH), 7.00 (1H, d, ArCH), 7.03 (1H, t, ArCH), 7.05 (2H, s, NH_2), 7.10–7.81 (2H, m, ArCH), 8.04 (2H, d, ArCH), 8.18 (1H, d, ArCH), 8.54 (1H, s, OH), 11.33 (1H, s, NH hydrazo form); ^{13}C NMR (DMSO-d_6, ppm) δ: 35.76 (CH pyran), 56.93 (CN), 108.44, 112.36, 114.13, 114.99, 115.21, 116.80, 117.02, 119.87, 128.10, 128.70, 128.82, 129.04, 129.18, 131.10, 133.36, 133.65, 135.65, 135.58, 137.19, 147.40, 153.41, 159.43 (ArCH), 194.83 (C = O). MS, m/z (%): 524 (M^+, 29.56) with a base peak at 324 (100).

2-Amino-6-[(2-benzoyl-4-nitrophenyl)azo]-7-hydroxy-4-(4-methoxyphenyl)-*4H*- chromene-3-carbonitrile (10c) Reddish orange solid (84%), m.p. 208 °C; IR (KBr) cm^{-1}: 3460 (OH), 3450, 3220 (NH_2), 2220 (CN), 1690 (CO), 1450 (N = N); ^1H NMR (DMSO-d_6, ppm) δ: 3.72 (3H, s, OCH_3), 4.65 (1H, s, CH pyran), 6.59 (1H, d, $J = 8.8$ Hz, Ar–CH), 7.01 (2H, s, NH_2), 7.07 (2H, d, $J = 8.8$ Hz, Ar–CH), 7.51 (2H, t, Ar–CH), 7.66 (1H, t, Ar–CH), 8.38 (1H, d, $J = 8.8$ Hz, Ar–CH), 8.46 (1H, s, Ar–CH), 8.51 (1H, d, $J = 8.8$ Hz, Ar–CH), 9.88 (1, s, OH), 11.59 (1H, s, NH hydrazo form); ^{13}C NMR (DMSO-d_6, ppm) δ: 35.63 (CH pyran), 55.06 (OCH_3), 57.47 (CN), 109.00, 113.16, 113.80, 119.34, 120.03, 121.15, 124.17, 126.26, 128.24, 128.85, 129.33, 133.78, 135.75, 136.94, 137.05, 137.46, 147.67, 152.18, 153.67, 155.49, 158.02, 159.25 (Ar-C), 194.35 (C = O). MS, m/z (%): 547 (M^+, 25.61) with a base peak at 334 (100).

2-Amino-6-[(2-benzoyl-4-nitrophenyl)azo]-7-hydroxy-4-(4-bromophenyl)-*4H*- chromene-3-carbonitrile (10d) Reddish orange solid (84%), m.p. 250 °C; IR (KBr) cm^{-1}: 3460 (OH), 3450, 3220 (NH_2), 2220 (CN), 1655 (CO), 1445 (N = N); ^1H NMR (DMSO-d_6, ppm) δ: 4.64 (1H, s, CH pyran), 6.59 (1H, d, $J = 8.8$ Hz, Ar–CH), 6.87 (2H, d, $J = 8.8$ Hz, ArCH), 6.96 (2H, d, $J = 8.8$ Hz, ArCH), 7.05 (2H, s, NH_2), 7.07 (2H, d, $J = 8.8$ Hz, Ar–CH), 7.51 (2H, t, Ar–CH), 7.66 (1H, t, Ar–CH), 7.72 (2H, d, $J = 8.4$ Hz, Ar–CH), 8.46 (1H, s, Ar–CH), 9.70 (1, s, OH), 11.45 (1H, s, NH hydrazo form); ^{13}C NMR (DMSO-d_6, ppm) δ: 36.83 (CH pyran), 55.06 (OCH_3), 57.47 (CN), 109.00, 113.16, 113.80, 119.34, 120.03, 121.15, 124.17, 126.26, 128.24, 128.85, 129.33, 133.78, 135.75, 136.94, 137.05, 137.46, 147.67, 152.18, 153.67, 155.49, 159.25 (Ar-C), 194.35 (C = O). MS, m/z (%): 595 (M^+, 31.5) with a base peak at 334 (100).

2-Amino-6-[(2-benzoyl-4-nitrophenyl)azo]-7-hydroxy-4-(4-chlorophenyl)-*4H*- chromene-3-carbonitrile (10e) Reddish orange solid (84%), m.p. 250 °C; IR (KBr) cm^{-1}: 3460 (OH), 3450, 3220 (NH_2), 2220 (CN), 1655 (CO), 1450 (N = N); ^1H NMR (DMSO-d_6, ppm) δ: 4.65 (1H, s, CH pyran), 7.05 (2H, s, NH_2), 6.25–8.85 (13H, m, ArCH), 9.85 (1H, s, OH), 11.59 (1H, s, NH hydrazo form): ^{13}C NMR (DMSO-d_6, ppm) δ: 36.83 (CH pyran), 57.47 (CN), 109.00, 113.16, 113.80, 119.34, 120.03, 121.15, 124.17, 126.26, 128.24, 128.85, 129.33, 133.78, 135.75, 136.94, 137.05, 137.46, 147.67, 152.18, 153.67, 155.49, 158.02, 159.25 (Ar-C), 194.35 (C = O). MS, m/z (%): 551 (M^+, 34.6) with a base peak at 335 (100).

Absorption, Distribution, Metabolism, Excretion, and Toxicity (ADMET) Predictions

The molecular structure of the examined candidates played a crucial task in deciding the ADMET properties and the pharmacokinetic etiquette. The ADMET predictions were done by exploiting the PreADMET software.

In-silico molecular docking studies

The In-silico docking strategy was recruited to perform structure based drug designing in order to procure the more effective inhibitors of GlcN-6-P and PI3K from the synthesized drug candidates. The ACD/Labs-Chemsketch program was utilized to create the 3D atomic coordinates of the ligands. 2VF5 and 2RD0 (PDB ID's), respectively, were reviewed as the most appropriate pure 3D crystal structure of the Glucosamine-6-phosphate of GlcN-6-P synthase and the p110α subunit of PI3K as fetched from the protein data bank (PDB) (Source: www.rcsb.org/pdb/). Energy of the molecules was minimized, using a Dundee PRODRG2 server, and was exploited to minimize the energy of the targeted ligands (Schüttelkopf and Aalten 2004). The docking simulations were prepared, ran, and analyzed by the means of the Graphical User Interface program, namely Autodock4 from "Auto-Dock Tools (ADT, 1.5.6)" (Morris et al. 1998).

The assignment of the Kollman united-atom charges along with the addition of the only polar hydrogens to the receptor protein was achieved. Ligands were assigned with the Gasteiger charge, and the torsions were set. The grids were made and adjusted in an X, Y, Z-axis so that it comprises the whole active site of the targeted proteins with a grid spacing of 0.375 Å. The Lamarckian Genetic Algorithm (LGA) was preferred over the Monte Carlo method, which is present in earlier versions of AutoDock. The docking specifications were stationed to the software's default values and a standard decorum was maintained and followed throughout the docking screenings. The result outcomes were elucidated on the basis of a pdf file generated by the software by ranking the different ligands with respect to the forecasted binding energy.

A cluster analysis, based on values of the root mean square deviation, was conducted. The minimum energy coordinates were ascertained, using the same rmsd table created in the dlg file. The cluster, securing the lowest energy, was appraised as the most reliable solution.

For 3D visualization of ligand protein interaction, we employed the UCSF Chimera 1.11.2 and mcule, a web interface, which uses the WebGL/Javascript based molecule viewer of GLmol.

Biological studies

Antimicrobial screening

The microorganism inoculums were uniformly spread using sterile cotton swabs on a sterile Petri dish malt extract agar (for fungi) and nutrient agar (for bacteria). One hundred

milliliters of each sample (at 10 mg/ml concentrations dissolved in Dimethyl Sulfoxide) was added to each well (6-mm-diameter holes were cut in the agar gel, 30 mm apart from one another). The samples were compared to the standard drug as positive control and DMSO solvent control. The cultures were incubated for 24 h at 37 °C (for bacteria) and for 48 h at 28 °C (for fungi). After incubation, the microorganism growth was observed. Inhibition zones of the bacterial and fungal growth were measured in millimeters. Tests were performed in triplicate (Cappuccino and Sherman 1999; Vanden-Berghe and Vlientinck 1991).

Cytotoxic screening

Human colon carcinoma (HCT-116), human hepatocellular carcinoma (HEPG-2), and human breast adenocarcinoma (MCF-7) cell lines were obtained from the American Type Culture Collection (ATCC, Rockville, MD). The cells were grown on RPMI-1640 medium supplemented with 10% inactivated fetal calf serum and 50 µg/mL gentamycin. The cells were maintained at 37 °C in a humidified atmosphere with 5% CO_2 and were subcultured two to three times a week. Potential cytotoxicity of the compounds was evaluated on tumor cells using the method of Gangadevi and Muthumary (Klancnik et al. 2010). The cells were grown as monolayers in growth RPMI-1640. The monolayers of 104 cells adhered at the bottom of the wells in a 96-well microtiter plate incubated for 24 h at 37 °C in a humidified incubator with 5% CO_2. The monolayers were then washed with sterile phosphate buffered saline (0.01 M pH 7.2) and simultaneously the cells were treated with different concentrations of tested sample (started from 500 µM) dissolved in DMSO. A control of untreated cells along with solvent control was made in the absence of tested sample. Positive controls containing doxorubicin were also tested as a reference drug for comparison. Six wells were used for each concentration of the test sample. After treatment 24 h, the number of the surviving cells was determined by staining the cells with crystal violet (Mosmann 1983; Gangadevi and Muthumary 2007) followed by cell lysing using 33% glacial acetic acid and reading the absorbance at 590 nm using microplate reader (SunRise, TECAN, Inc, USA) after well mixing. The absorbance values from untreated cells were considered as 100% proliferation. The number of viable cells was determined using microplate reader and the percentage of viability was calculated as [1-(ODt/ODc)]×100% where ODt is the mean optical density of wells treated with the tested sample and ODc is the mean optical density of untreated cells. The relation between surviving cells and drug concentration was plotted to get the survival curve of each tumor cell line after treatment with the specified compound. The 50% inhibitory concentration (IC50), the concentration required to cause toxic effects in 50% of intact cells, was estimated from graphic plots.

Compliance with ethical standards

Conflict of interest The authors declare that they have no conflict of interest.

Publisher's note: Springer Nature remains neutral with regard to jurisdictional claims in published maps and institutional affiliations.

References

Afifi TH, Okasha RM, Ahmed HEA, Ilaš J, Saleh T, Abd-El-Aziz AS (2017) Structure-activity relationships and molecular docking studies of chromene and chromene based azo chromophores: A novel series of potent antimicrobial and anticancer agents. Excli J. 16:868–902

Afifi TH, Okasha RM, Alsherif H, Ahmed HEA, Abd-El-Aziz AS (2017) Design, synthesis, and docking studies of 4h-chromene and chromene based azo chromophores: a novel series of potent antimicrobial and anticancer agents. Curr Org Synth. 14:1036–1051

Ali KA, Abdelhafez NAA, Ragab EA, Ibrahim AA, Amr AE (2015) Design and synthesis of novel fused heterocycles using 4-chromanone as synthon. Russ J Gen Chem. 85:2853–2860

Alley MC, Scudiero DA, Monks A, Hursey ML, Czerwinski MJ, Fine DL, Abbott BJ, Mayo JG, Shoemaker RH, Boyd MR (1988) Feasibility of Drug Screening with Panels of Human Tumor Cell Lines Using a Microculture Tetrazolium Assay. Cancer Res. 48:589–601

Atta-ur-Rahman MIC, Thomsen WJ (2001) Bioassay techniques for drug development bioassay techniques for drug development. Harwood Academic Publishers, Amsterdam

Bejan V, Mantu D (2012) Mangalagi II. Ultrasound and microwave assisted synthesis of isoindolo-1,2-diazine: a comparative study. Ultrason Sonochem. 19:999–1002

Boominathan M, Nagaraj M, Muthusubramanian S, Krishnakumar RV (2011) Efficient atom economical one-pot multicomponent synthesis of densely functionalized 4H-chromene derivatives. Tetrahedron 67:6057–6064

Bruce NA, Gurney EG, James AM, Bartsch H (1973) Carcinogens as Frameshift Mutagens: Metabolites and Derivatives of 2-acetylaminofluorene and other Aromatic Amine Carcinogens. PNAS 69:3128–3213

Cai SX, Drewe J, Kasibhatla S (2006) A chemical genetics approach for the discovery of apoptosis inducers: from phenotypic cell based HTS assay and structure-activity relationship studies, to identification of potential anticancer agents and molecular targets. Curr Med Chem. 13:2627–2644

Cappuccino JG, Sherman N (1999) Microbiology: A Laboratory Manual. Benjamin-Cummings Pub Co., California

Chen-Chen M, Zhao-Peng L (2016) Design and synthesis of coumarin derivatives as novel PI3K inhibitors. Anticancer agents Med Chem. 17:395–403

Cheng JF, Ishikawa A, Ono Y, Arrhenius T, Nadzan A (2003) Novel chromene derivatives as TNF-alpha inhibitors. Bioorg Med Chem Lett. 13:3647–3650

Chmara H, Andruszkiewicz R, Borowski E (1984) Inactivation of glucosamine-6-phosphatesynthetase from Salmonella typhimurium LT2 SL 1027 by N-beta-fumarylcarboxyamido-l-2,3-

diamino-propionic acid. Biochem Biophys Res Commun. 120:865–872
El-Agrody AM, Al-Dies AM, Fouda AM (2014) Microwave assisted synthesis of 2-amino-6-methoxy-4H-benzo[h]chromene derivatives. Eur J Chem. 5:133–137
Elinson MN, Ilovaisky AI, Merkulova VM, Belyakov PA, Chizhov AO, Nikishin GI (2010) Solvent-free cascade reaction: Direct multicomponent assembling of 2-amino-4H-chromene scaffold from salicylaldehyde, malononitrile or cyanoacetate and nitroalkanes. Tetrahedron 66:4043–4048
Engelman JA (2009) Targeting PI3K signalling in cancer: Opportunities, challenges and limitations. Nat Rev Cancer 9:550–562
Fadda AA, Berghot MA, Amer FA, Badawy DS, Bayoumy NM (2012) Synthesis and antioxidant and antitumor activity of novel pyridine, chromene, thiophene and thiazole derivatives. Arch Pharm Chem. 345:378–385
Foroumadi A, Emami S, Sorkhi M, Nakhjiri M, Nazarian Z, Heydar S, Ardestani S, Poorrajab F, Shafiee A (2010) Chromene-based synthetic chalcones as potent antileishmanial agents: synthesis and biological activity. Chem Biol Drug Des. 75:590–596
Gangadevi V, Muthumary M (2007) Preliminary studies on cytotoxic effect of fungal taxol on cancer cell lines. Afr J Biotechnol. 6:1382–1386
Govori S, Haziri A, Ademi K, Neziraj N (2017) Molecular docking studies of fused coumarin derivatives as inhibitors of GlcN-6. J Environ Sci Health. 52:1041–1045
Hamelin J, Bazureau JP, Texier-Boullet F (2002) Microwaves in organic synthesis. Wiley-VCH: Weinheim, Germany, p 253.
Hermanson D, Addo S, Bajer A, Marchant J, Das S, Srinivasan B, AlMousa F, Michelangeli F, Thomas D, LeBien T, Xing C (2009) Dual mechanisms of sha 14-1 in inducing cell death through endoplasmic reticulum and mitochondria. Mol Pharmacol. 76:667–678
Hosseini-Sarvari M, Shafiei Haghighi S (2011) Multi-component synthesis of 2-amino-4H-chromenes catalyzed by nano ZnO in water. Collect Czechoslov. Chem Commun. 76:1285–1298
Hou TJ, Zhang W, Xia K, Qiao XB, Xu XJ (2004) ADME Evaluation in drug discovery. 5. correlation of caco-2 permeation with simple molecular properties. J Chem Inf Comput. Sci. 44:1585–1600
Irvine JD, Takahashi L, Lockhart K, Cheong J, Tolan JW, Selick HE, Grove R (1999) MDCK (Madin-Darby Canine Kidney) cells: a tool for membrane permeability screening. J Pharm Sci. 88:28–33
Kasibhatla S, Gourdeau H, Meerovitch K, Drewe J, Reddy S, Qiu L, Zhang H, Bergeron F, Bouffard D, Yang Q (2004) Discovery and mechanism of action of a novel series of apoptosis inducers with potential vascular targeting activity. Mol Cancer Ther. 3:1365–1373
Kirilmis C, Ahmedzade M, Servi S, Koca M, Kizirgil A, Kazaz C (2008) Synthesis and antimicrobial activity of some novel derivatives of benzofuran: Part 2. The synthesis and antimicrobial activity of some novel 1-(1-benzofuran-2-yl)-2-mesitylethanone derivatives. Eur J Med Chem. 43:300–308
Klancnik A, Piskernik S, Jersek B, Mozina SS (2010) Evaluation of diffusion and dilution methods to determine the antibacterial activity of plant extracts. J Microbiol Methods. 81:121–126
Lather A, Sharma S, Khatkar A (2018) Virtual screening of novel glucosamine-6-phosphate synthase inhibitors. Comb Chem High Throughput Screen. 21:182–193
Lee K-S, Khil L-Y, Chae S-H, Kim D, Lee B-H, Hwang G-S, Moon C-H, Chang T-S, Moon C-K (2006) Effects of DK-002, a synthesized(6aS,cis)-9,10-Dimethoxy-7,11b-dihydro-indeno[2,1-c] chromene-3,6a-diol, on platelet activity. Life Sci. 78:1091–1097
Liu JL, Gao GR, Zhang X, Cao SF, Guo CL, Wang X, Tong LJ, Ding J, Duan WH, Meng LH (2014) DW09849, A selective phosphatidylinositol 3-kinase (pi3k) inhibitor, prevents pi3k signaling and preferentially inhibits proliferation of cells containing the oncogenic mutationp110 (H1047R). J Pharmacol Exp Ther. 348:432–441
Makarem S, Mohammadi AA, Fakhari AR (2008) A multi-component electro-organic synthesis of 2-amino-4H-chromenes. Tetrahedron Lett. 49:7194–7196
Ma X, Chen C, Yang J (2005) Predictive model of blood-brain barrier penetration of organic compounds. Acta Pharm Sin. 26: 500–512.
Mannhold R (2008) Molecular Drug Properties: Measurement and Prediction; Wiley-VHC Verlag GmbH & Co. KGaA: Weinheim, Germany, p. 30.
Mao X, Cao B, Wood TE, Hurren R, Tong J, Wang X, Wang W, Li J, Jin Y, Sun W, Spagnuolo PA, MacLean N, Moran MF, Datti A, Wrana J, Batey RA, Schimmer AD (2011) A small-molecule inhibitor of D-cyclin transactivation displays preclinical efficacy in myeloma and leukemia via phosphoinositide 3-kinase pathway. Blood. 117:1986–1997
Marshall NJ, Andruszkiewicz R, Gupta S, Milewski S, Payne JW (2003) Structure activity relationships for a series of peptidomimetic antimicrobial prodrugs containing glutamine analogues. J Antimicrob Chemother. 51:821–831
Mehrabi H, Kazemi-Mireki M (2011) CuO nanoparticles: an efficient and recyclable nanocatalyst for the rapid and green synthesis of 3,4-dihydropyrano[c]chromenes. Chin Chem Lett. 22:1419–1422
Morris GM, Goodsell DS, Halliday RS, Huey R, Hart WE, Belew KR, Olson AJ (1998) Automated docking using a lamarckian genetic algorithm and empirical binding free energy function. J Comput Chem. 19:1639–1662
Mosmann T (1983) Rapid colorimetric assay for cellular growth and survival: application to proliferation and cytotoxicity assays. J Immunol Methods. 65:55–63
Mukohara T (2015) PI3K Mutations in breast cancer: prognostic and therapeutic implications. Breast Cancer (Dove. Med. Press) 7:111–123
Nareshkumar J, Jiayi X, Ramesh MK, Fuyong D, Guo JZ, Emmanuel P (2009) Identification and structure-activity relationships of chromene-derived selective estrogen receptor modulators for treatment of postmenopausal symptoms. J Med Chem. 52:7544–7569
Safari J, Javadian L (2015) Ultrasound assisted the green synthesis of 2-amino-4H-chromene derivatives catalyzed by Fe_3O_4-functionalized nanoparticles with chitosan as a novel and reusable magnetic catalyst. Ultrason Sonochem. 22:341–348
Sashidhara KV, Kumar M, Modukuri RK, Srivastava A, Puri A (2011) Discovery and synthesis of novel substituted benzocoumarins as orally active lipid modulating agents. Bioorg Med Chem Lett. 21:6709–6713
Schüttelkopf AW, Aalten DM (2004) PRODRG: A tool for high-throughput crystallography of protein-ligand complexes. Acta Cryst. 60:1355–1363
Tanaka JCA, da Silva CC, Ferreira ICP, Machado GMC, Leon LL, de Oliveira AJB (2007) Antileishmanial activity of indole alkaloids from Aspidospermaramiflorum. Phytomedicine. 14:377–380
Tiana D, Dasa S, Doshia J, Pengb J, Linb J, Xing C (2008) sHA 14-1, a stable and ROS-free antagonist against anti-apoptotic Bcl-2 proteins, bypasses drug resistances and synergizes cancer therapies in human leukemia cell. Cancer Lett. 259:198–208
Vanden-Berghe DA, Vlientinck AJ (1991) Screening Methods for Antibacterial and Antiviral Agents from Higher Plants. In: Hostettmann K (ed.) Methods in plant biochemistry vi. assays for bioactivity. Academic Press, London, p 47–69
Wainwright M (2008) Dyes in the development of drugs and pharmaceuticals. Dyes Pigments. 76:582–589

Widelski J, Popova M, Graikou K, Glowniak K, Chinou I (2009) Coumarins from Angelica lucida L. antibacterial activities. Molecules. 14:2729–2734

Yadav JS, Reddy BVS, Gupta MK, Prathap I, Pandey SK (2007) Amberlyst A-21®: an efficient, cost-effective and recyclable catalyst for the synthesis of substituted 4H-chromenes. Catal Commun. 8:2208–2211

Yuan TL, Cantley LC (2008) PI3K Pathway alterations in cancer: variations on a theme. Oncogene. 27:5497–5510

Zbancioc G, Mangalagiu II (2006) Microwave-assisted synthesis of highly fluorescent pyrrolopyridazine derivatives. Synlett. 5:804–806

Zbancioc G, Zbancioc AM (2014) Mangalagiu II. Ultrasound and microwave assisted synthesis of dihydroxyacetophenone derivatives with or without 1,2-diazine skeleton. Ultrason Sonochem. 21:802–811

Zhao L, Vogt PK (2008) Class I PI3K in oncogenic cellular transformation. Oncogene. 27:5486–5496

Zhao YH, Le J, Abraham MH, Hersey A, Eddershaw PJ, Luscombe CN, Boutina D, Beck G, Sherborne B, Cooper I (2010) Evaluation of human intestinal absorption data and subsequent derivation of a Quantitative Structure-Activity Relationship (QSAR) with the abraham descriptors. J Pharm Sci. 90:749–784.